Sol−Gel Fabrication and Electrical Property of Nanocrystalline $(RE_2O_3)_{0.08}(ZrO_2)_{0.92}$ (RE = Sc, Y) Thin Films

Y. W. Zhang, Y. Yang, S. Jin, S. J. Tian, G. B. Li, J. T. Jia, C. S. Liao, and C. H. Yan*

State Key Lab of Rare Earth Materials Chemistry and Applications & PKU-HKU Joint Lab on Rare Earth Materials and Bioinorganic Chemistry, Peking University, Beijing 100871, China

Received June 27, 2000. Revised Manuscript Received November 2, 2000

Dense, crack-free, and homogeneous nanocrystalline $(RE_2O_3)_{0.08}(ZrO_2)_{0.92}$ (RE = Sc, Y) thin films (≈0.58-μm thick) on monocrystalline silicon (100) wafers were fabricated by a simple sol−gel spin-coating method under reduced annealing temperature and were characterized by X-ray diffraction (XRD), scanning electron microscopy (SEM), atomic force microscopy (AFM), Auger electron spectroscopy (AES), and impedance studies. Some key correlative processing parameters such as coating solution composition and gel-firing temperature have been optimized. XRD results indicate that the as-fabricated $(Sc_2O_3)_{0.08}(ZrO_2)_{0.92}$ thin films can achieve good crystallization in a pure cubic phase at a relatively low annealing temperature not exceeding 800 °C in 2 h and the nanocrystal size grows with elevation of the annealing temperature. AFM and SEM micrographs show that the $(RE_2O_3)_{0.08}(ZrO_2)_{0.92}$ nanocrystals after undergoing annealing at 950 °C for 2 h are uniform in the size range of 50−60 nm. AES profile analysis suggests that the $(Sc_2O_3)_{0.08}(ZrO_2)_{0.92}$ thin films are fairly pure with good composition homogeneity in the depth range of 75−500 nm. Impedance measurements reveal that the oxide ion conductivity of the nanocrystalline thin films is 10 times higher than that of the respective bulk material at temperatures beyond 600 °C. A decrease of grain boundary resistance related to interfacial effects is predominately responsible for this electrical conductivity enhancement.

Introduction

As essential parts of fuel cells and oxygen sensors, electrolyte thin films are required to be denser, thinner, more homogeneous, and more ion-conductive so as to reduce the overall resistance and finally the operating temperature of these devices. Normally, these requirements can be met by improving the fabrication techniques and hence electrical properties of the as-used films. For decades, more and more techniques including the sol−gel method,[1−3] spray pyrolysis,[4] chemical vapor deposition (CVD),[5] RF sputtering,[6] reactive magnetron co-sputtering,[7] electrochemical vapor deposition (EVD),[8] and plasma spraying[9] have been explored for fabricating these thin films with specific thicknesses and microstructures. Among these techniques, sol−gel processing can offer an advantage of fabricating oxide thin films with a wide range of compositions in improved homogeneity and high purity at relatively low temperature over the other fabrication techniques.

Previously, much attention in this regard has been paid to thin films of yttria-stabilized zirconia (YSZ).[1−5,7,9] So far, little attention has been paid to fundamental studies on nanocrystalline scandia-stabilized zirconia (ScSZ) thin films mainly because of the application limitation caused by the higher cost of scandia than that of yttria. Recently, it seems that the high cost could be considerably reduced with an advanced scandium separation technique[10] if commercial demand for scandia greatly increases. As is well-known, $(Sc_2O_3)_{0.08}(ZrO_2)_{0.92}$-(8ScZr) polycrystalline material holds the highest electrical conductivity among all the zirconia-based electrolytes.[11] This provides a unique possibility for lowering the operating temperature of the electrochemical devices if ScSZ thin films could be fabricated with superior quality and were taken in these devices like YSZ thin films were.

The electrical properties of YSZ thin films deposited by the as-listed techniques were mostly reported to be

* To whom correspondence should be addressed. Fax: +86-10-6275-4179. E-mail: chyan@chem.pku.edu.cn.

(1) Xia, C. R.; Cao, H. Q.; Wang, H.; Yang, P. H.; Meng, G. Y.; Peng, D. K. *J. Membr. Sci.* **1999**, *162*, 181.
(2) S.-Lee, J.; Matsubara, T.; Sei, T.; Tsuchiya, T. *J. Mater. Sci.* **1997**, *32*, 5249.
(3) Chen, C. C.; Nasrallah, M. M.; Anderson, H. U. *Solid State Ionics* **1994**, *70/71*, 101.
(4) Matsuzaki, Y.; Hishinuma, M.; Yasuda, I. *Thin Solid Films* **1999**, *340*, 72.
(5) Wang, H. B.; Xia, C. R.; Meng, G. Y.; Peng, D. K. *Mater. Lett.* **2000**, *44*, 23.
(6) Gharbage, B.; Mandier, F.; Lauret, H.; Roux, C.; Pagnier, T. *Solid State Ionics* **1995**, *82*, 85.
(7) Horita, S.; Watanabe, M.; Umemoto, S.; Masuda, A. *Vacuum* **1998**, *51*, 609.
(8) Ioroi, T.; Hara, T.; Uchimoto, Y.; Oguchi, Z.; Takehara, Z. *J. Electrochem. Soc.* **1997**, *144*, 1362.
(9) Chiodelli, G.; Magistris, A.; Scagliotti, M.; Parmagiani, F. *J. Mater. Sci.* **1988**, *23*, 1159.
(10) Yan, C. H.; Zhang, Y.; Liao, C. S.; Wei, Z. J.; Zhang, Y. W.; Li, B. G. Patent of P. R.C., 1127791, July 31, 1996.
(11) Badwal, S. P. S. *Solid State Ionics* **1992**, *52*, 23.

10.1021/cm0005236 CCC: $20.00
Published on Web 01/12/2001

similar to those of the corresponding bulk material.[2,3,9] More recently, a considerable enhancement of ionic conduction in the sol−gel-derived nanocrystalline $(Y_2O_3)_{0.08}(ZrO_2)_{0.92}$(8YZr)[12] and $SrCe_{0.95}Yb_{0.05}O_3$ (refs 13 and 14) thin films on an Al_2O_3 substrate was reported by Kosacki and Anderson. On the other hand, there were some interesting reports about the electrical properties of nanocrystalline oxide bulk materials. Ramamoorthy et al. noticed that the total electrical conductivity is mainly influenced by the grain boundaries in the $(Y_2O_3)_x(ZrO_2)_{1-x}$ ($x = 0.02-0.12$) ultrafine-grained material.[15] Mondal et al. reported an enhanced specific grain boundary conductivity in nanocrystalline $(Y_2O_3)_x(ZrO_2)_{1-x}$ ($x = 0.017, 0.029$) bulk material, which was ascribed to low Si content and its grain size-dependent segregation in the samples.[16] Demetry and Shi found that nanocrystalline TiO_2 has enhanced conductivity and a lower specific grain boundary resistivity with respect to microcrystalline TiO_2.[17] Apparently, these latest findings admit that the electrical properties of solid oxides are highly correlative with the grain size variation from microcrystalline to nanocrystalline.

Of course, to know the transport properties of ScSZ and YSZ thin films on alternate substrates in the nanometer regime and the relationship between properties and microstructures are very attractive because of the applicable potential of these films in the electrochemical devices.

One year ago, our laboratory successfully developed a modified Pechini-type sol−gel process by which dense and crack-free nanocrystalline thin films of rare earth doped $CoFe_2O_4$ (ref 18) and $La_{1-x}Sr_xMnO_3$ (ref 19) could be fabricated on dense substrates. The objectives of this study are to use the sol−gel method to prepare nanocrystalline 8ScZr and 8YZr thin films on monocrystalline silicon (100) wafers at a reduced annealing temperature, to explore their electrical properties, and to correlate the properties to their microstructures. For comparison, microcrystalline 8ScZr bulk material has also been made. The sol−gel-derived films were characterized by X-ray diffraction (XRD), scanning electron microscopy (SEM), atomic force microscopy (AFM), Auger electron spectroscopy (AES), and impedance studies. In this paper, the research results on sol−gel fabrication and electrical properties of nanocrystalline $(RE_2O_3)_{0.08}(ZrO_2)_{0.92}$ (RE = Sc, Y) thin films are presented.

Experimental Section

Sol−Gel Preparation. A sol−gel process similar to that used in our laboratory[18,19] was used in this study. All the used chemical reagents contain trace Al and Si impurities (<100 ppm). The coating solution was prepared by dissolving rare earth nitrate (99.95−99.99%) and zirconium oxochloride hydrate (A.R.) at a given molar ratio and a certain amount of poly(ethylene glycol) (C.R., molecular weight: ≈20 000) in an appropriate amount of ethanol−water solvents. Then, it was stirred for 2 h before filtration. To avoid precipitation, the pH value of the solution was maintained below 1.5 by adding drops of concentrated nitric acid. From the as-prepared coating solution, thin films were deposited on the clean monocrystalline silicon (100) wafers through repetition of the cycle of spin-coating (at a speed of 4000 rpm for 8 s), drying (at 110 °C for 20 min), and gel-firing (at 400 °C for 30 min). To achieve good crystallization, the sol−gel-derived thin films were annealed at the temperatures of 600−950 °C for 2 h in an oxygen-flow atmosphere.

Characterization Methods. The as-given molar ratio of metal ions was standardized by an inductively coupled plasma atomic emission spectrometer (Leeman Lab. Inc.). The gel decomposition behavior was investigated with a thermal analyzer (DuPont 2100) in air at a heating rate of 15 °C/min, using α-Al_2O_3 as a reference. The phase formation of nanocrystals was identified by an X-ray powder diffractometer (Rigaku D/max-2000) using Cu Kα radiation ($\lambda = 1.5408$ Å). The thin film thickness was determined by SEM (AMARY 1910FE), and its surface structures were probed by both SEM and AFM (Auto Probe CP, PSI). The surface and bulk composition of the films were studied by an Auger electron spectroscope (PHI-610) under the primary electron-beam energy of 3.0 keV and the emission current of 25 mA. The depth profile was measured by using argon ion sputtering at the speed of 25 nm/min.

Electrical Property Measurements. The electrical properties of the thin films were determined in air by ac two-probe measurements on a frequency response analyzer (HP-4192A LF, 200 Hz to 12 MHz).[20] The impedance data points were collected with a temperature interval of 40 °C upon cooling over the temperature range of 1000−400 °C. With Pt paste (TR-7902, Tanaka Kikinzoku) two Pt lead electrodes were adhered to two cross sections (0.5 × 0.05 cm) of the sample with an interelectrode area of 1 × 0.5 cm and then the paste was fired at 950 °C for 30 min. The net impedance of the thin films Z_f was calculated from the following expression,

$$\frac{1}{Z - Z_e} = \frac{1}{Z_f} + \frac{1}{Z_s - Z_e}$$

where Z is the total impedance of the sample, Z_e is the impedance of the electrode lead, and Z_s is the impedance of the substrate. The electrical conductivity of the nanocrystalline thin films and the polycrystalline material was calculated from the interceptions of the observed semicircle on the real axis of the Cole−Cole plot.

Results and Discussion

Optimization of Fabrication Processing. According to the Pechini-type sol−gel process,[21] chelate ligands such as citric acid were used to coordinate with the metal ions so as to keep them from hydrolyzing and to esterify with ethylene glycol catalyzed by slightly concentrated mineral acid. Then, the resulting intermediate was polymerized upon heating to form viscous solution. Recently, Peng et al.[22] and our laboratory modified this process, the research results showing that dense and crack-free nanocrystalline oxide thin films could be fabricated from the coating solution containing poly(ethylene glycol) in no need of esterification. In this

(12) Kosacki, I.; Gorman, B.; Anderson, H. U. In *Ionic and Mixed Conductors*; Ramanarayanan, T. A., Worrell, W. L., Tuller, H. L., Kandkar, A. C., Mogensen, M., Gopel, W., Eds.; The Electrochemical Society: Pennington, NJ, 1998; Vol. 3, p 631.
(13) Kosacki, I.; Anderson, H. U. *Appl. Phys. Lett.* **1996**, *69*, 4171.
(14) Kosacki, I.; Anderson, H. U. *Solid State Ionics* **1997**, *97*, 429.
(15) Ramamoorthy, R.; Sundararaman, D.; Ramasamy, S. *Solid State Ionics* **1999**, *123*, 271.
(16) Mondal, P.; Klein, A.; Jaegermann, W.; Hahan, H. *Solid State Ionics* **1999**, *118*, 331.
(17) Demetry, C.; Shi, X. L. *Solid State Ionics* **1999**, *118*, 271.
(18) Cheng, F. X.; Peng, Z. Y.; Xu, Z. G.; Liao, C. S.; Yan, C. H. *Thin Solid Films* **1999**, *339*, 109.
(19) Yan, C. H.; Huang, Y. H.; Wang, Z. M.; Zhu, T.; Liao, C. S.; Cheng, F. X.; Zhang, Z. L.; Xu, G. X. *Thin Solid Films* **2000**, *366*, 302.
(20) Bauerle, J. E. *J. Phys. Chem. Solids* **1969**, *30*, 2657.
(21) Pechini, M. P. U.S. Patent, 3330697, July 11, 1967.
(22) Peng, Z. Y.; Li, X.; Zhao, Y. M.; Cai, H.; Zhao, S. Q.; Hu, G. D.; Xu, B. K. *Thin Solid Films* **1996**, *286*, 270.

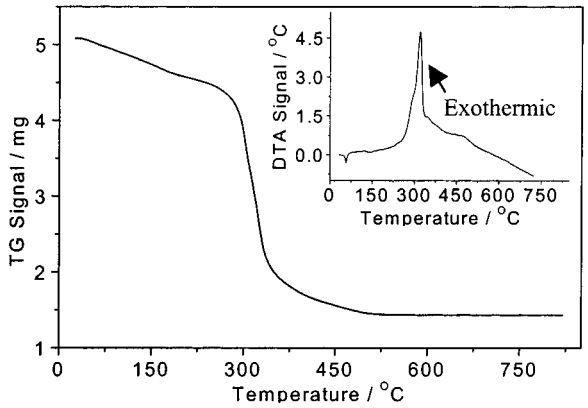

Figure 1. A combined TG-DTA run of the dried gel.

research, when following this modified process, we found that citric acid could precipitate the Zr^{4+} ions in the coating solution; thus, it was excluded. In experiment, the influences of coating solution compositions and gel-firing temperature on the 8ScZr thin film formation have been investigated in the case of nonexistence of chelate ligands.

Spin-coating of the precursor solutions containing metal ions (C_M = 0.1 M) and PEG (C_{PEG} = 40 mg/mL) on Si substrates showed that the as-deposited films tend to be easier to combine with the substrate and appear smoother as the alcohol−water volume ratio R was raised from 5:1 to 8:1. This is probably accounted for in the stronger intermolecular bonding and affinity with the Si substrate in ethanol than in water. Experimentally, the maximum ratio of R is reached at 8:1.

The gel-firing temperature was observed to have effects on the film quality. When 300 °C was taken as the gel-firing temperature, the five-layer thin film prepared from the coating solution (C_M = 0.1 M, C_{PEG} = 40 mg/mL, and R = 8:1) showed many cracks and pinholes after annealing at 850 °C. However, when 400, 500, and 600 °C were taken as the gel-firing temperatures, respectively, all the as-made five-layer thin films are flat, crack-free, and specular after annealing at 850 °C. The results could be understood by the TG-DTA curve of the gel decomposition, as shown in Figure 1. The gel can completely decompose below 500 °C. During the decomposition of PEG, a large exothermic effect in the temperature range of 200−400 °C was produced. Under 400 °C, the unfinished gel decomposition is expected to result in a great deal of organic impurities in the microstructures of the resin intermediate of the thin film. When the thus-made thin film was annealed at high temperature, the impurities will be burnt out with the release of some gas byproducts promptly. Hence, the gas eruption will make the thin film form cracks and pinholes easily. Of course, with little impurities left by the gel fired beyond 400 °C, the as-annealed thin film will not be easily cracked. For operation convenience, we select 400 °C as the gel-firing temperature. In this case, the elemental analysis evidenced that organic contaminants in the fired gel are tiny (found: C, 4.00%; H, 1.31%; N, <0.3%).

Previous studies revealed that PEG concentration was closely connected with the sol−gel-derived film property.[18] Too low PEG concentration would produce thin films with many pinholes, whereas too high PEG concentration would greatly increase the roughness of the thin films. In the present case, the influences of PEG content with a narrow range of 20−60 mg/mL in the coating solution (R = 8:1 and C_M = 0.1 M) on the root-mean-square roughness R_{rms} and the film thickness H were estimated by AFM and SEM. The root-mean-square roughness R_{rms} is given by the standard deviation of the data from the AFM image and defined by the following expression,

$$R_{rms} = \sqrt{\frac{\sum_{n=1}^{N}(z_n - \bar{z})^2}{N-1}}$$

where z_n represents the height of the nth data point, $\bar{z}$ is equal to the mean height of Z_n in AFM topology, and N is the number of data points. Table 1 summarizes the values of R_{rms} and H for 8ScZr thin films annealed at 950 °C. Therein, n denotes the coating layer number.

Table 1. R_{rms} and H Values for the 8ScZr Thin Films Prepared from Different Coating Solutions (Annealing at 950 °C, n = 20)

C_{PEG} (mg/mL)	20	40	60	C_M (M)	0.05	0.10	0.15
H (nm)	304	295	307	H (nm)	157	295	461
R_{rms} (nm)	2.35	2.90	2.39	R_{rms} (nm)	2.32	2.90	3.63

Table 1 shows that 8ScZr thin films have not displayed significant difference in the values of H and R_{rms} when C_{PEG} is increased from 20 to 60 mg/mL. This means that the as-given PEG concentration range is appropriate in the present case. Referring to our previous work,[18,19] C_{PEG} = 40 mg/mL was taken in the coating solutions.

The metal ion concentration in the coating solution is another key parameter of the sol−gel process. When C_{PEG} = 40 mg/mL and R = 8:1 are sustained, the values of R_{rms} and H of the 8ScZr thin films prepared from the solutions containing various metal concentrations are also obtained by AFM and SEM and listed in Table 1. The table indicates that R_{rms} and H of the 8ScZr thin films increase with increasing C_M from 0.05 to 0.15 M. This can be attributed to the amount of increase of the metal ions enclosed in the network constructed by the deposited PEG polymers. Additionally, we observed that the deposited film thickness per layer will be reduced and pinholes are easier to be produced in the case of too low metal concentration, and the films will become rougher and cracks are easier to be formed in the case of too high metal concentration. Therefore, a compromised choice is taking medium metal ion concentration. Herein, C_M is optimized to 0.1 M. Under this condition, the maximal coating layer number for the crack-free 8ScZr thin films can reach 47. However, the film roughness increases with increasing its thickness. Hence, the most favored coating layer number should be less than 40.

Annealing Behaviors. Figure 2 shows the phase development of the as-prepared 8ScZr thin films at various annealing temperatures. The broadening of the diffraction peaks indicates the presence of 8ScZr nanocrystals at an annealing temperature as low as 600 °C for 2 h. These nanocrystals could achieve good crystallization in a pure cubic structure beyond 800 °C. This good-crystallization temperature is about 600 °C lower than that of the polycrystalline pellets prepared by the

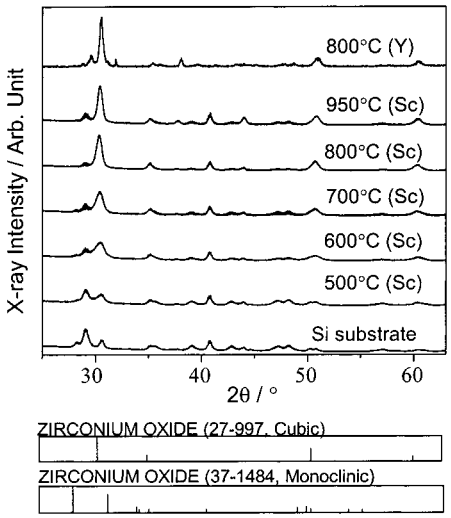

Figure 2. XRD patterns of the 8ScZr thin film as a function of annealing temperature.

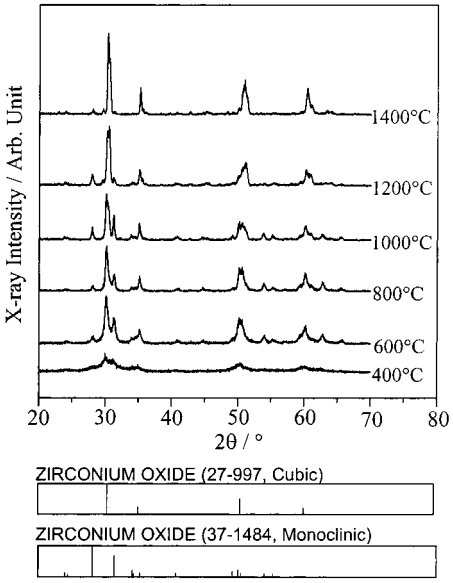

Figure 3. XRD patterns of the sol−gel-derived 8ScZr polycrystalline sample as a function of sintering temperature.

same gel. Figure 3 shows the XRD profiles of the bulk material as a function of the sintering temperature. It is found that the bulk sample can attain nearly pure cubic crystallization after sintering at 1400 °C for 24 h. Below 1400 °C the sample contains quite a few monoclinic ZrO_2 grains, whose amount decreases with increasing sintering temperature. The nanocrystalline 8YZr thin films are also yielded in a pure cubic phase (also shown in Figure 2).

Generally, the nanocrystal size can be estimated from the Scherrer equation,

$$D = \frac{k\lambda}{\beta \cos \theta}$$

where k is a constant, θ and β are the diffraction angle and full-width at half-maximum (fwhm) of an observed peak, respectively, and D is the average grain size. In the calculation, $k = 0.90$ and β of the (111) peak at $2\theta = 30.5°$ was taken. The calculated results show that 8ScZr nanocrystals gradually grow from 10 to 20 nm as the annealing temperature is elevated from 600 to

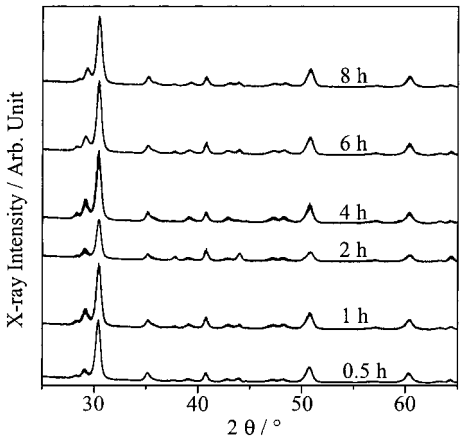

Figure 4. XRD patterns of the 8ScZr thin films as a function of annealing time.

950 °C. Such a grain growth is a common phenomenon in the annealing behavior of the film or powder. Figure 4 displays the time dependence of the XRD pattern for the nanocrystalline 8ScZr thin films annealed at 950 °C. It seems that well-crystallized nanocrystals in the cubic phase can be gained in less than half an hour; thus, 2 h is adequate for the film annealing. It is also observed that the fwhm of the (111) diffraction peak changed little with extending the annealing time from 0.5 to 8 h. This suggests that the length of annealing time has no obvious effects on the nanocrystal size in the present case.

On the basis of the as-optimized parameters and annealing conditions, a series of dense and crack-free nanocrystalline thin films of rare earth doped zirconia such as $(Sc_2O_3)_x(ZrO_2)_{1-x}$ ($x = 0.02-0.24$), $(Sc_2O_3)_{0.08-x}$-$(Y_2O_3)_x(ZrO_2)_{0.92}$ ($x = 0.02-0.08$), $(Y_2O_3)_{0.10}(ZrO_2)_{0.90}$, $(Sc_2O_3)_{0.08}(Al_2O_3)_x(ZrO_2)_{0.92-x}$ ($x = 0.05-0.15$), and $(RE_2O_3)_{0.08}(ZrO_2)_{0.92}$ (RE = La, Nd, Sm, Gd, Dy, Ho, Er, Tm, Yb, and Lu) have been successfully fabricated in this research. Typically, Figure 5 exhibits the cross section (a) and surface (b) SEM micrographs of the 8ScZr thin films after 30 spin-coating cycles and annealing at 950 °C for 2 h. Figure 6 depicts the surface AFM micrographs of the 8ScZr (a) and 8YZr (b) thin films. The thickness of the deposited films are determined to be $\approx 0.58\ \mu$m from the cross-section SEM photo. As seen from the surface micrographs, the nanocrystals of 8ScZr and 8YZr thin films appear dense and uniform with an average grain size of 50 and 55 nm, respectively. Because smaller nanograins contribute more to the broadening of the diffraction peaks, the average nanocrystal size estimated from the Scherrer equation is smaller than that determined from AFM topology in the case of 8ScZr films.

For comparison 8ScZr polycrystals were prepared by the coprecipitation method. After sintering at 1600 °C for 24 h took place, the polycrystals in predominately the cubic phase with an average grain size of 2.9 μm were yielded.

Film Composition Characterization. Figure 7 shows a surface AES spectrum of the films after annealing at 950 °C for 2 h. Only Zr, Sc, and O atoms were detected with some carbon atoms. Because the carbon AES profile became very weak after Argon ion sputtering for 1 min, the carbon atoms can be ascribed to the surface contaminants coming from the storage

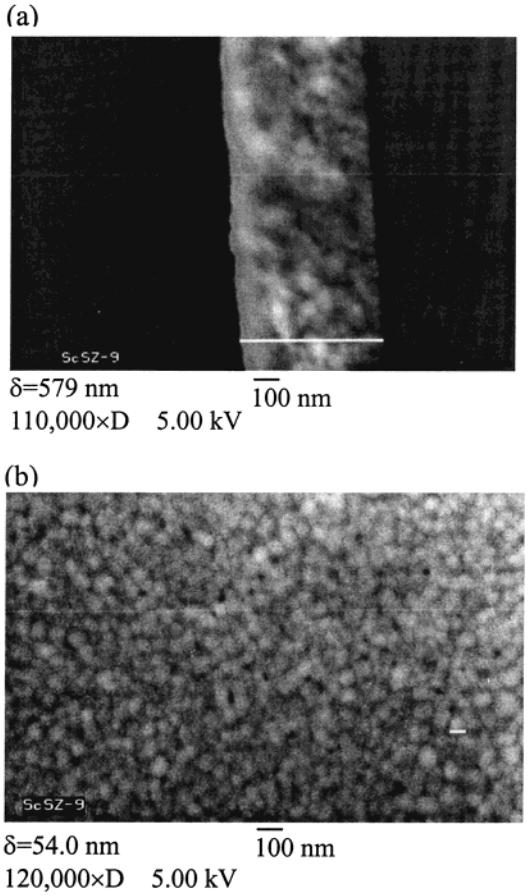

Figure 5. Cross-section (a) and surface (b) SEM micrographs of the 8ScZr thin films after annealing at 950 °C for 2 h.

or determination environment. Hence, the purity of the deposited films is fairly high. Figure 8 displays the in-depth AES composition profile as a function of sputtering time or depth. It is observed that the atomic ratio of Sc:Zr:O stay nearly unchanged at 1:3.5:5.7 in the depth range of 75−500 nm and the interdiffusion layer thickness is <100 nm. These results mean that our fabrication process offers a good composition homogeneity despite the ratio to some extent deviating from the theoretical ratio of 1:5.75:13, owing to the measuring method. From Figure 8 it is also noted that the determined Si percentage appears to be zero in the surface and nearly a constant value of ≈15% across the film thickness from 75 to 500 nm. It indicates that such a high Si concentration is caused neither by its interdiffusion from the substrate to the thin film nor by its trace content in the starting materials but attributed to the experimental errors coming from the overlapping of the Si peak with the Zr satellite peak with the electron kinetic energy of ≈92 eV. If the interference of the Zr element on the determination of Si content can be eliminated, it is rational that the as-made thin films contain trace Si element across the thickness below 500 nm.

Electrical Properties. Figure 9 depicts the impedance spectra of the nanocrystalline 8ScZr and 8YZr thin films and 8ScZr bulk material. At 472 °C (Figure 9a), the impedance spectrum of the 8ScZr bulk material exhibits three semicircles corresponding to bulk resistance (>3.32 MHz), grain boundary resistance (6.20 kHz to 3.32 MHz), and electrode reaction impedance (<6.20

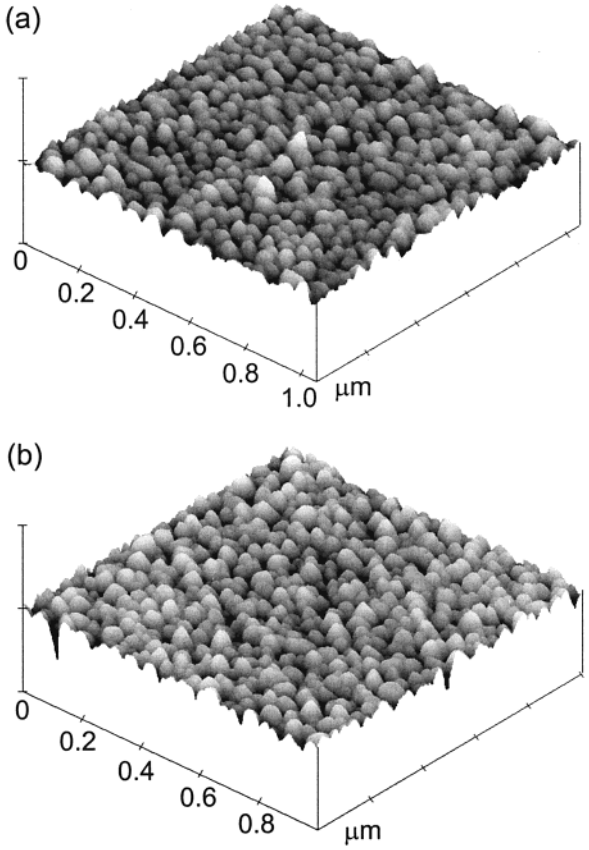

Figure 6. Three-dimensional AFM micrographs of nanocrystalline 8ScZr (a) and 8YZr (b) thin films deposited on Si(100) substrate after annealing at 950 °C for 2 h.

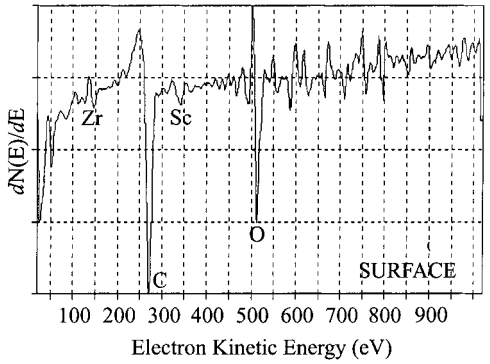

Figure 7. Surface Auger electron spectrum of the 8ScZr thin films after annealing at 950 °C for 2 h.

kHz), respectively. In the impedance spectrum of the 8ScZr bulk material at 930 °C (Figure 9b), although the high-frequency semicircle (>1.69 MHz) is correlative with both bulk and grain boundary resistance, the bulk resistance governs the electrical conductivity as previously revealed.[23] In the case of the thin films, the impedance spectra at 930 °C (Figure 9c) showed one high-frequency semicircle for 8ScZr (>80.8 kHz) and for 8YZr (>140 kHz), respectively. The impedances at low frequency are ascribed to the diffusion process of Warburg impedance of the interface.[20]

As determined from the Arrhenius plot of log σT versus $1/T$ (shown in Figure 10), the conductivity activation energies are 1.13 and 1.28 eV for the 8ScZr

(23) Aoki, M.; Chiang, Y.-M.; Kosacki, I.; J.-R. Lee, L.; Tuller, H. L.; Liu, Y. P. *J. Am. Ceram. Soc.* **1996**, *79*, 1169.

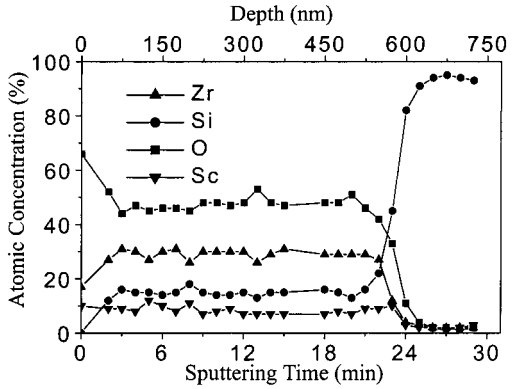

Figure 8. In-depth AES compositional profile of the 8ScZr thin films after annealing at 950 °C for 2 h.

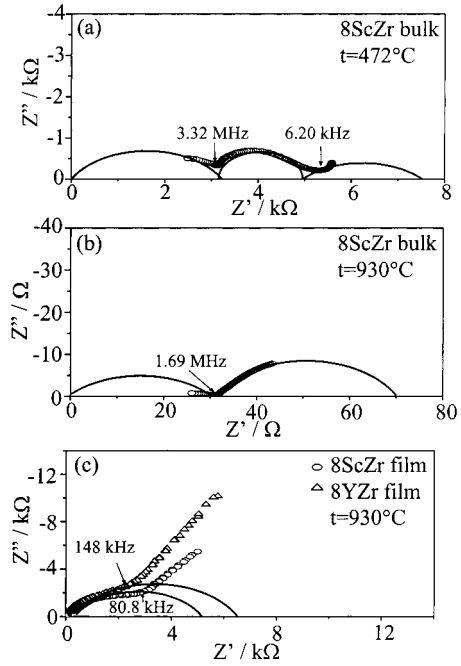

Figure 9. Impedance spectra of 8ScZr bulk material at 472 (a) and 930 °C (b) and that of nanocrystalline 8ScZr and 8YZr thin films at 930 °C (c).

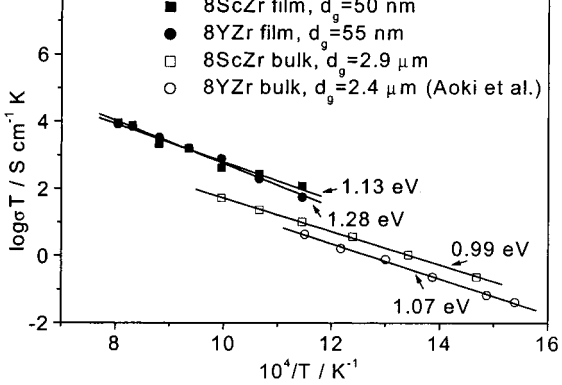

Figure 10. Arrhenius plot for the electrical conductivity of nanocrystalline 8ScZr and 8YZr thin films and the corresponding bulk materials.

and 8YZr thin films, respectively, and 0.99 and 1.07 eV for the 8ScZr and 8YZr[23] bulk materials, respectively. It is also noted that the electrical conductivity of the thin films at temperatures beyond 600 °C is 10 times higher than bulk electrical conductivity of the bulk

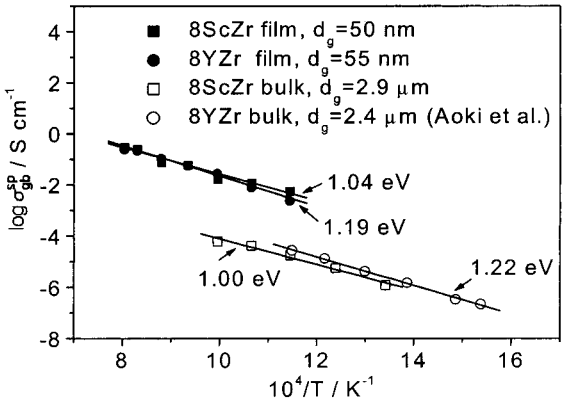

Figure 11. Arrhenius plot for the specific grain boundary conductivity of nanocrystalline 8ScZr and 8YZr thin films and the corresponding bulk materials.

materials. Therefore, the as-described differences in conductivity activation energy and electrical conductivity strongly suggested that the high-frequency semicircles in nanocrystalline 8ScZr and 8YZr thin films are predominately attributed to the grain boundary resistance.[12] Moreover, if this were not the case, there would exist a significant difference of electrical conductivity between nanocrystalline 8ScZr and 8YZr thin films because the electrical conductivity of 8ScZr bulk is much higher than that of 8YZr bulk at a given temperature. The attribution can also be somewhat understood from Ramamoorthy et al.'s results in the $(Y_2O_3)_x(ZrO_2)_{1-x}$ ($x = 0.02-0.12$) ultrafine-grained material, according to which the grain boundaries have a dominate effect on the total electrical conductivity.[15]

Figure 11 shows the logarithm of the specific grain boundary conductivity σ_{gb}^{sp} versus $1/T$ for the nanocrystalline 8ScZr and 8YZr thin films and their bulk materials. σ_{gb}^{sp} corresponding to a single grain boundary was previously defined as follows,

$$\sigma_{gb}^{sp} = \sigma_{gb}^{T}(\delta_{gb}/d_g)$$

where σ_{gb}^{T} is the total grain boundary conductivity, d_g is the grain size, and δ_{gb} is the thickness of the grain boundary, which was assumed to be 2 nm in the ZrO_2 system.[23]

As displayed in Figure 11, the conductivity activation energy for the grain boundary conductivity of the 8ScZr and 8YZr thin films are consistent with that of the corresponding bulk materials. This result quite approves the above-made assertion; that is, the grain boundary effect is predominately responsible for the high-frequency semicircle in the impedance spectra of the nanocrystalline thin films. It can also be observed from Figure 11 that the electrical conductivity values of the thin films greatly increase when compared with those of the bulk materials. This enhancement could be interpreted in terms of the size-dependent grain boundary impurity segregation, as suggested by Aoki et al.[23] Similar enhancements were ever observed in nanocrystalline 8YZr[12] and $SrCe_{0.95}Yb_{0.05}O_3$ (refs 13 and 14) thin films, nanocrystalline $(Y_2O_3)_x(ZrO_2)_{1-x}$ ($x = 0.017$, 0.029),[16] TiO_2 (ref 17) and CeO_2,[24] and microcrystalline $(CaO)_{0.015}(ZrO_2)_{0.85}$.[23]

(24) Chiang, Y.-M.; Lavik, E. B.; Kosacki, I.; Tuller, H. L.; Ying, J. Y. *Appl. Phys. Lett.* **1996**, *69*, 185.

To date, evidence has been still inadequate for us to clarify the source of enhanced ionic conduction in nanocrystalline materials. [25] In the present case, maybe the electrical conductivity is greatly enhanced due to the fact that the nonstoichometry level of the thin films is significantly raised by the interfacial effects between grains and grain boundaries. The interfacial effects will become prominent with the sharp increases of grain boundaries as the grain size is reduced to the nanometer regime.

Conclusions

Dense, crack-free, and homogeneous nanocrystalline $(Sc_2O_3)_{0.08}(ZrO_2)_{0.92}$ and $(Y_2O_3)_{0.08}(ZrO_2)_{0.92}$ thin films have been successfully fabricated by a simple sol−gel process. In this method, metal ions can homogeneously mix with PEG and are included in the polymer-constructed network through intermolecular bonding in the coating solution. Hence, this processing allows us conveniently to prepare well-crystallized rare earth stabilized zirconia thin films at reduced annealing temperature with low cost, in the case of the precursor solution undergoing neither chelation nor esterfication before spin-coating. The as-deposited thin films show an enhanced ionic conduction at temperatures beyond 600 °C, predominately due to the decrease of grain boundary resistance related to the interfacial effects. Such an enhancement has promised that both ScSZ and YSZ thin films are good candidates for electrolyte in electrochemical devices.

Acknowledgment. Grants-in-aid from NSFC (29525101, 29701001, 29832010, and 20023005), the State Key Project for Fundamental Research of MOST (G1998061300), the Training Project for Doctoral Student of MOE, and Founder Group Corporation Foundation of Peking University are gratefully acknowledged. The authors also thank Dr. X. P. Jing for his very helpful discussions on the impedance data of the samples.

CM0005236

(25) Tuller, H. L. *Solid State Ionics* **2000**, *131*, 143.